Soft Matter

www.rsc.org/softmatter

Volume 9 | Number 33 | 7 September 2013 | Pages 7879–8074

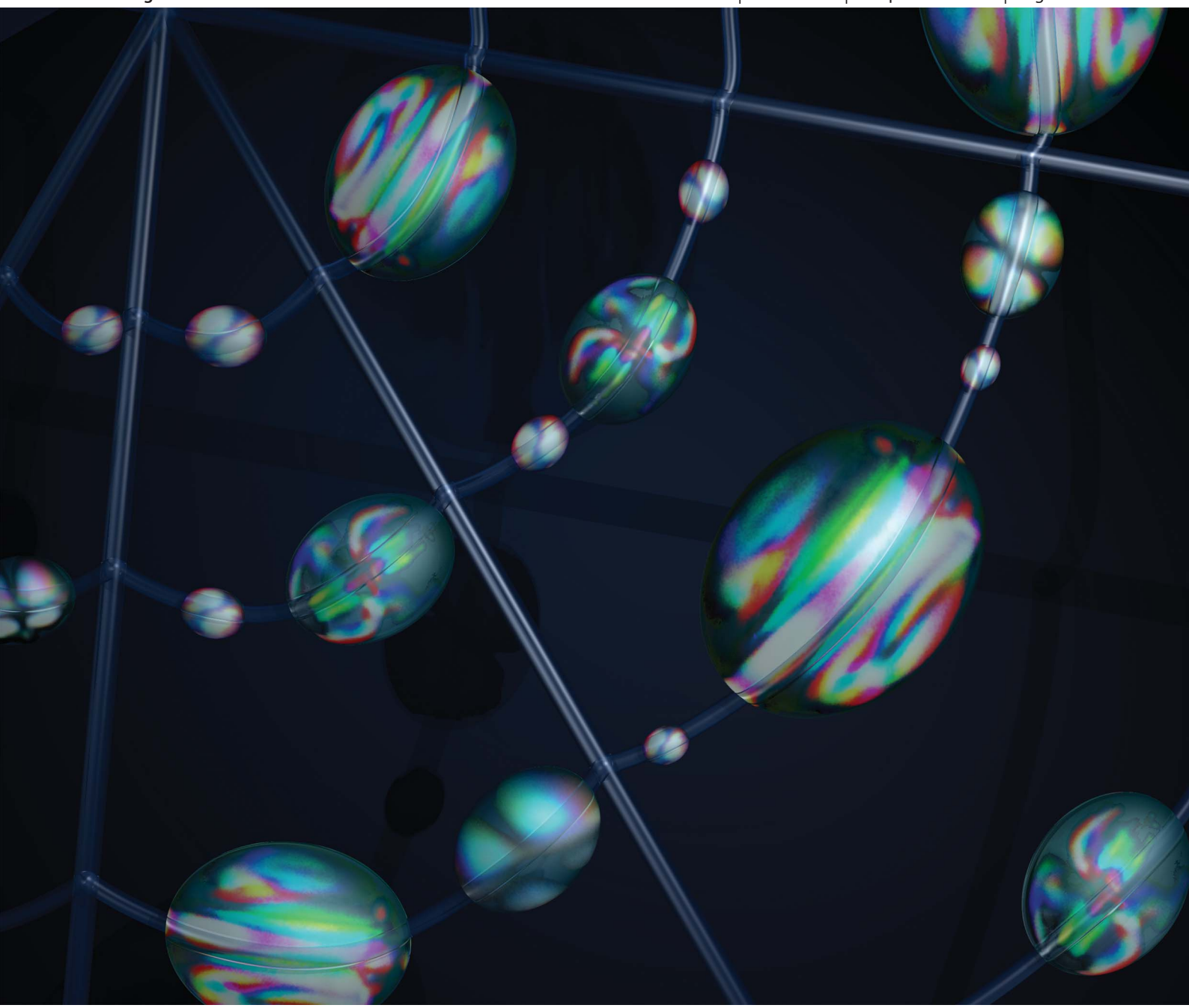

ISSN 1744-683X

RSC Publishing

PAPER

Slobodan Žumer, Maria H. Godinho *et al.*

Liquid crystal necklaces: cholesteric drops threaded by thin cellulose fibres

1744-683X(2013)9:33;1-2

Soft Matter

RSC Publishing

PAPER

Liquid crystal necklaces: cholesteric drops threaded by thin cellulose fibres†

Cite this: *Soft Matter*, 2013, **9**, 7928

Yong Geng,[a] David Seč,[b] Pedro L. Almeida,[ac] Oleg D. Lavrentovich,[d] Slobodan Žumer*[bef] and Maria H. Godinho*[a]

Received 1st April 2013
Accepted 21st May 2013

DOI: 10.1039/c3sm50900a

www.rsc.org/softmatter

Liquid crystals in confined geometries exhibit numerous complex structures often including topological defects that are controlled by the nematic elasticity, chirality and surface anchoring. In this work, we study the structures of cholesteric droplets pierced by cellulose fibres with planar anchoring at droplet and fibre surfaces. By varying the temperature we demonstrate the role of twisting power and droplet diameter on the equilibrium structures. The observed structures are complemented by detailed numerical simulations of possible director fields decorated by defects. Three distinct structures, a bipolar and two ring configurations, are identified experimentally and numerically. Designing cholesteric liquid crystal microdroplets on thin long threads opens new routes to produce fibre waveguides decorated with complex microresonators.

Introduction

Soft matter systems characterized by inherently strong susceptibility to external stimuli are emerging as promising materials for applications in photonics and lasing. Particularly important are liquid crystals (LCs) with their optical anisotropy and ability to shape and direct light. From the standpoint of photonic and lasing applications, it is convenient to distinguish two classes of LCs, namely, (i) intrinsically periodic chiral mesophases and strongly confined LCs that both can possess a photonic bandgap for visible light, and (ii) LC composites such as colloidal particles assembled into a periodic structure in a LC host that exhibit Bragg type light scattering. Here we restrict our attention to the former systems.

The lasing in planar liquid crystalline geometries was predicted already in the early seventies, but it was experimentally realized about ten years later.[1] For more details see reviews by Coles and coworkers devoted to planar geometries.[2,3] Though liquid–crystalline structures appearing after confinement to droplets[4] and after application of external fields[5] are well known, recent research demonstrates new opportunities, such as whispering gallery modes in LC droplets used as microresonators.[6,7]

Cholesteric liquid crystal droplets offer an especially rich spectrum of possibilities as they exhibit various structures controlled by chirality of constituent molecules (that establishes intrinsic periodicity), bulk elasticity and anisotropic surface energy.[8,9] Droplets with concentric packing of cholesteric layers can be used as tunable onion-like Bragg microresonators.[10–12] The cholesteric droplets, prepared as polymer dispersed liquid crystals (PDLC),[13] can also be used for lasing.[14] Although liquid crystal based microresonator structures are experimentally achievable, their coupling to other photonic elements is still a work in progress. Among recently proposed promising sophisticated structures are nematic shells,[15] handle bodies[16] and LC necklaces.[17,18] In the latter case, the nematic droplets are threaded by a cellulose fibre, which offers an interesting possibility for the coupling of optical fibres to LC droplet resonators. This idea stimulated our interest in cholesteric droplets threaded by a fibre. The chiral cholesteric phase offers more possibilities for the realization of a tunable microresonator as compared to a simple nematic.

In this paper we examine cholesteric structures in droplets located on a cylindrical fibre that goes through the axis of the droplet and thus makes its topology very different from that of the previously studied spherical droplets.[17] The experimental study, based on polarizing optical microscopy (POM), is complemented by numerical simulations of structures and their POM appearance. The approach is based on our recent detailed analysis of cholesteric droplet structures.[9] The piercing fibre changes not only the topology of the droplet, but also distorts the spherical shape to an approximately ellipsoidal droplet and

[a]*CENIMAT/I3N, Departamento de Ciênciados Materiais, Faculdadede Ciências e Tecnologia, FCT, Universidade Nova de Lisboa, 2829-516 Caparica, Portugal. E-mail: mhg@fct.unl.pt; y.geng@fct.unl.pt; Tel: +351 212948564*

[b]*Faculty of Mathematics and Physics, University of Ljubljana, 1000 Ljubljana, Slovenia. E-mail: slobodan.zumer@fmf.uni-lj.si; david.sec@fmf.uni-lj.si*

[c]*Área Departamental de Física, Instituto Superior de Engenharia de Lisboa, ISEL, Instituto Politécnico de Lisboa, R. Conselheiro Emídio Navarro, 1, 1950-062 Lisboa, Portugal. E-mail: palmeida@adf.isel.pt; Tel: +351 21218317135*

[d]*Liquid Crystal Institute and Chemical Physics Interdisciplinary Program, Kent State University, Kent, Ohio 44242, USA. E-mail: olavrent@kent.edu*

[e]*Center of Excellence NAMASTE, Jamova 39, 1000 Ljubljana, Slovenia*

[f]*Jozef Stefan Institute, Jamova 39, 1000 Ljubljana, Slovenia*

† Electronic supplementary information (ESI) available: Movies S1 and S2. See DOI: 10.1039/c3sm50900a

adds an additional cylindrical surface with planar anchoring along the droplet's long axis. We demonstrate that the presence of the fibre stabilizes three distinguishable structures identified experimentally and numerically. Finally, the effects of temperature dependent chirality and droplet size on the structures and stability are explored.

Experimental details and results

To produce the cholesteric system, we used the nematic liquid crystal *4′-n-pentyl-4-cyanobiphenyl* (5CB) and the chiral nematic compound *(S)-4′-(3-methylpentyl)-4-cyanobiphenyl* (5CB*). 5CB* presents a chemical structure very similar to that of 5CB, and a 10% (w/w) mixture of 5CB* in 5CB (5CB*Mix) was chosen to produce a helical pitch p_0 detectable by POM. 5CB* presents a N* phase between −14 °C and −22 °C and a helical pitch of about 0.3 μm, and a smectic A phase is reported for temperatures below −22 °C.[19] The LC chiral mixture, 5CB*Mix, presents an I–N* phase transition at 28.3 °C and a pitch value of 7 μm measured by optical microscopy, at room temperature (∼19 °C). The 5CB* compound was synthesized according to the procedure described in detail in ref. 20. The nematic liquid crystal 5CB used exhibits a nematic phase in the temperature range from 18 °C to 34 °C.

Cellulose fibres were prepared from 60% (w/w) hydroxypropylcellulose (HPC) (Aldrich, $\overline{M_w}$ = 100.000 g mol^{-1}; molar substitution, $\overline{M_s}$ = 3.5, as determined by ^{1}H NMR) solutions in dimethylacetamide (DMac) (Riedel-de Haen, 99%). The viscous iridescent solution in the nematic chiral phase was poured into a 1 ml syringe (diameter 4.5 mm) fitted with a 27-gauge needle (diameter 0.2 mm) which was then placed on the infusion syringe pump (KDS100) to control the polymer solution feed rate. A conducting ring, 15 cm in diameter, was held coaxially with the needle tip at its center, and electrically connected to it. Both the needle and the ring were directly connected to the positive output of a high voltage supply (Glassman EL 30 kV). After applying the electric potential between the metallic syringe-tip and the plate, the polymeric solution was continuously fed to the syringe-tip at a constant flow rate of 0.04 ml h^{-1}, and accelerated by the ensuing electric field towards a collector consisting of two conductive strips separated by a void gap of 0.5 cm. The optimized operating conditions for the continuous drawing of cellulose derivative fibres were a voltage of 15 kV for a distance between the nozzle and the collector of l = 15 cm. In general, fibres get thinner at higher accelerating voltage; however, several other parameters (such as the solution viscosity, needle diameter and the distance to the target) also contribute to the fibre shape and dimensions.[21] In order to obtain uniaxially aligned fibre arrays, a specially designed fibre collector made of two parallel aluminium strips stuck together by two conductive aluminium wires was used. Each aluminium strip had a length of 2 cm and a width of 0.2 cm. The distance between metallic strips was 1 cm (see Fig. 1a). After electrospinning, the HPC fibre arrays deposited across the aluminium strips form suspended arrays. The fibres were then carefully dried under vacuum, at room temperature, for 72 h before further characterization.

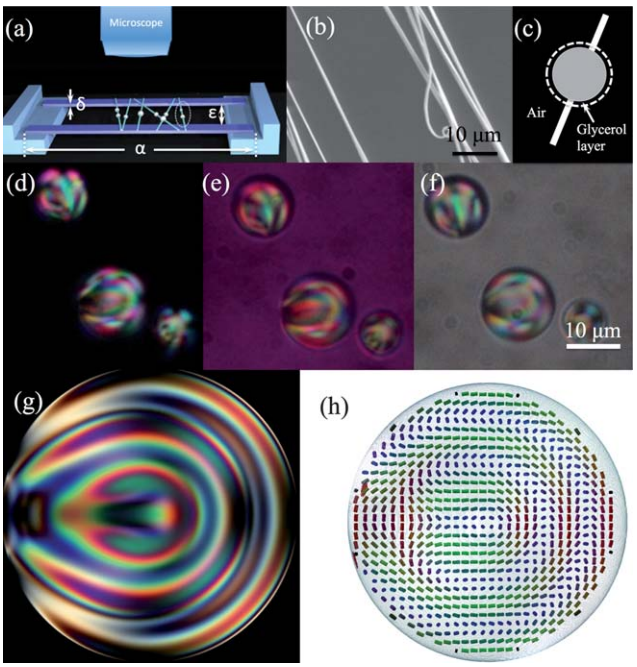

Fig. 1 Scheme of the sample holder and samples. (a) Scheme of the drops threaded on the fibres, which are supported by two parallel metal strips: α = 2 cm, δ = 0.2 cm and ε = 1 cm. (b) SEM picture of the electrospun fibres. (c) A sketch of a pierced LC droplet enclosed by a thin glycerol layer, which ensures planar anchoring conditions at the LC/air interface. (d) Crossed polarizers POM pictures of 5CB*Mix droplets dispersed in glycerol, (e) with an additional 530 nm quarter wavelength retardation plate, (f) under parallel polarizers. (g) Simulated polarization micrograph of the radial spherical structure and (h) the corresponding simulated director field.

Optical micrographs were taken using a transmission mode microscope, Olympus BH, equipped with polarizers, a camera and a heating/cooling stage (Mettler, FP90). The fibres were characterized by Scanning Electron Microscopy (SEM) using a SEM DSM962 model from Zeiss. Gold was deposited on the samples by sputtering in an Ar atmosphere, using a 20 mA current, for 30 seconds at a deposition rate of 3 Å s^{-1}. Images were obtained for an acceleration voltage of 5 kV. Fibre diameters and lengths were determined using *Image J* image processing software (version 1.40e). Blender, version 2.57b, was used to draw the 3D scheme. Photographs and movies were taken with a Canon EOS 550D coupled to the microscope through a LM-Scope adapter.

To generate stable planar anchoring at the cholesteric droplet surface we mixed 5CB*Mix with glycerol[4] (around 10% (w/w)) and we used ultrasound excitation in order to emulsify the system into small droplets (see Fig. 1d). The droplets were then carefully collected by a metallic wire (0.1 mm) at room temperature (∼19 °C) and transferred to suspended fibres assembled by electrospinning, as shown in Fig. 1a and c. In order to obtain well-dispersed and symmetrical droplets confined on the fibres (1–2 μm), the samples were heated to 80 °C for 5 minutes. The cellulosic fibres enforce tangential alignment along the fibre axis for 5CB molecules[17] (contrasting with the homeotropic alignment at the 5CB–air interface[22]). The p_0 value of 5CB*Mix increases from 7 μm at room temperature to 8 μm at T = 27.8 °C. The droplets with planar anchoring and

diameters from 15 μm to 40 μm, before being collected on the fibres, were examined between cross and parallel polarizers and by using a 530 nm retardation plate inserted between crossed polarizers at a 45° position (Fig. 1d–f). These observations reveal a characteristic cholesteric structure, which was imposed by the boundary conditions (Fig. 1g and h).

The cholesteric necklaces consist of drops suspended on fibres stretched in air (Fig. 1c). The drops retain a coverage by a thin layer of glycerol that keeps planar anchoring of the confined liquid crystal as is clearly observed under a polarizing microscope. Our liquid crystalline droplets satisfy the constraint $R \gg K/W$ for strong anchoring (strength W and Frank elastic constant K for the 5CB–glycerol system and the liquid crystal within the droplet will satisfy the boundary conditions[17]). Typical examples of two ellipsoidal droplets suspended on a microfibre, with 27 μm and 18 μm major axis, are given in Fig. 2. In Fig. 3 two different droplets show a series of dark and bright domains, which change color by crossed polarizers rotation, indicating the presence of concentric cylindrical cholesteric layers. By reducing the size of the drop relative to the cholesteric pitch, the configuration changes from a bipolar to a ring structure, as shown by images in Fig. 2 and 3.

In order to investigate how the ring defect structure (observed for droplets with structures similar to those shown in Fig. 2ii) evolves toward the final equilibrium configuration in the middle of the droplet, we heat the LC gradually above the cholesteric-to-isotropic transition to obtain the disordered state (at the rate of 1 °C min^{-1}; see also Movie S1 in the ESI,† which shows the heating process). In the heating process, the starting ring defect, located at the centre of the drop, starts to increase its diameter, as shown in Fig. 4i ($t = 2$ s), and close to this defect two symmetric black spots can be observed. For $t > 2$ s, the anisotropy inside the droplet starts to vanish asymmetrically relatively to the fibre main axis. This can be due to the twisting of the nematic layers. By cooling the droplet back to the cholesteric mesophase (Fig. 4ii and Movie S2 in the ESI,† which show the cooling process), we follow the generation and transformation of the structure that appears in the droplet. After 21 s the central ring defect reappears from the shrinking of a black region. Eventually, the initial state is reproduced, which is a strong proof that for such drops the ring structure is the most stable.

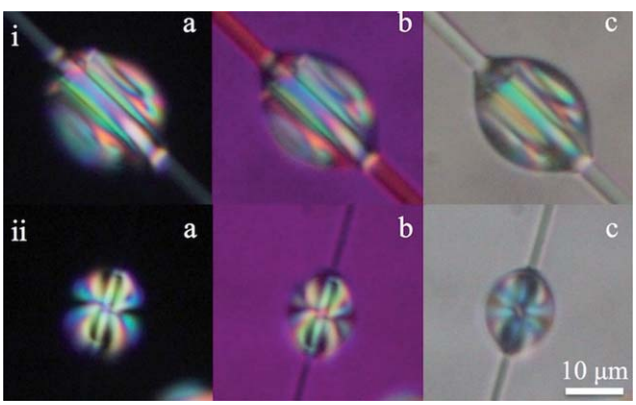

Fig. 2 Cholesteric bead textures observed by POM. (i) The bipolar structure with cylindrical cholesteric layers; (ii) smaller cholesteric bead with a totally different distribution of the director – the ring structure. The photos were taken (a) under the crossed polarizers, (b) with a 530 nm quarter wavelength retardation plate, between crossed polarizers, and (c) under parallel polarizers.

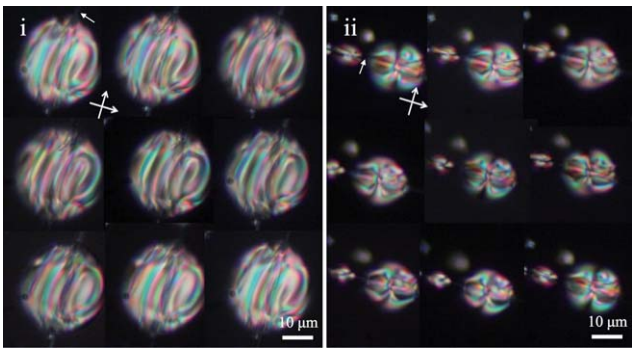

Fig. 3 POM pictures of cholesteric LC droplets, with different diameters, threaded by thin cellulose fibres with planar anchoring at the fibre surface and air interface. (i) A bigger and more spherical droplet exhibits a structure resembling a bipolar one in Fig. 2i. Note bent cholesteric layers due to a relatively stronger effect of the curved spherical surface. (ii) The ring structure resembling the ones in Fig. 2ii. In (i) and (ii) the cross polarizers were rotated 20° from picture to picture. The white arrows indicate the cellulosic microfibres piercing the droplets.

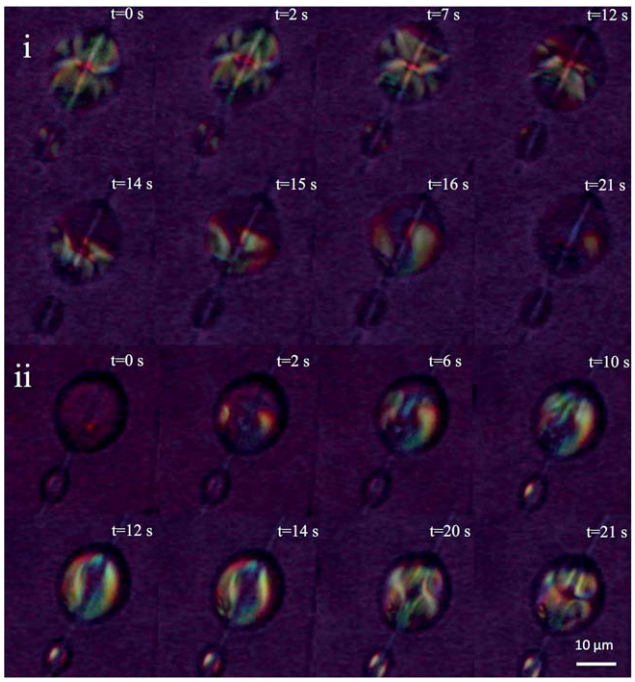

Fig. 4 Heating and cooling processes of a ring structure cholesteric droplet. (i) Snapshot images of the droplet evolution from the equilibrium director configuration ($t = 0$ s) to the isotropic phase ($t = 21$ s). The initial ring defect at the center of the drop ($t = 0$ s) first increases the diameter ($t = 2$ s) and then the ring defects increase their separation. (ii) When cooling the droplet from the isotropic phase ($t = 0$ s) back to the equilibrium ring configuration ($t = 21$ s), firstly the initial isotropic configuration transforms into a transient axial drop ($t = 14$ s) and eventually develops ring defects at the centre of the droplet around the fibre at $t = 21$ s. Snapshots were taken using a 530 nm quarter wavelength retardation plate between two crossed polarizers. The heating and cooling rates are both equal to 1 °C min^{-1}.

Numerical modelling and discussion

Here we start with a brief repetition of main configurations that appear in dispersed spherical cholesteric droplets. Director fields and defects are predominantly controlled by the boundary conditions and the twisting power qR with R being the radius of drops and $q = 2\pi/p_0$ the inverse cholesteric pitch.[9] Initial modelling of cholesteric droplets[8,23,24] with degenerate planar anchoring provided only general features of structures. Recent numerical modelling based on the minimization of the Landau-de Gennes free energy, which allows a detailed description of structures, unveiled a number of peculiarities in the defect regions.[9] For low twisting powers ($qR < 2\pi$), the stable droplet configuration is the bipolar structure (BS, see Fig. 4a in ref. 9), with two surface boojums positioned diametrically. The boojums are connected along the diameter of the droplet by a non-singular disclination with winding number +1 (cholesteric λ^{+1} line[25]). For higher twisting power values, $qR > 2\pi$, the bipolar structure continuously evolves into the radial spherical structure (RSS), which is the only one also observed in our dispersed cholesteric droplets (Fig. 1c–g). The RSS is characterized by a helicoidal winding of the λ^{+1} disclination into a double helix structure that spans from the centre of the droplet to the surface and ends with two singular +1 surface boojums, topologically equivalent to those in the BS. The RSS is thus notably different from the Frank-Pryce model structure[26] where a singular line with winding number +2 spans from the centre of the droplet to the surface. Among these two ground states of spherical cholesteric droplets, many intricate metastable states that differ in the topological defects and director fields can appear.[9] It is worth mentioning the diametrical spherical structure (DSS) with a cylindrical symmetry that is metastable because it consists of a series of ring defects around the symmetry axis (see Fig. 2a in ref. 9). The director field can be visualized as a sequence of concentrically positioned tori of deformed double twist cylinders with cross-sections being rather of the banana shape instead of being circular.

In the bipolar structure, the director field in the central region is predominantly in the direction of the escaped disclination. One could thus expect that piercing such droplets with cylindrical microfibres that prefer planar surface orientation would stabilize the bipolar structure. However, the inclusion of such additional surfaces changes also the droplet shapes. Since the nematic elasticity is typically much weaker than the surface tension,[27] the interfacial energy is thus expected to govern the shape of the threaded droplets. The typical experimental value for the surface tension of the LC–glycerol interface is $\sigma \sim 0.02\ \mathrm{J\ m^{-2}}$.[28] A similar order of magnitude of σ is expected for the LC–air[29] and LC–solid interface. Since the typical estimate for the elastic constant K of a LC is 5 pN, the ratio K/σ, which has the dimension of length, is very small, at a few nanometers. It implies that the shape of the threaded droplets that are larger than a few nanometers is controlled mainly by the surface tension rather than by the elastic energy. The high wettability of the cellulose fibres (low contact angle) provokes a change of the spherical shape to an approximately ellipsoidal form. Such deformed shapes could stabilize states that are otherwise metastable. Due to the planar requirements at the surface of the microfibre inside the ellipsoidal droplet, the preferred structures are expected to be close to the BS and DSS, both having a central region that would be the least frustrated by a fibre. Therefore, we used the director field Ansätze of the BS and DSS[9] as initial conditions in the numerical modelling of threaded droplets. We obtained three distinct structures: the bipolar structure (see Fig. 5a) and two ring structures (Fig. 5b and c). The bipolar structure is essentially the same as BS in spherical droplets with no additional inclusions. It is characterized by the cylindrical symmetry of the director field around the fibre, twisting only in the radial direction perpendicularly from the fibre. It has no bulk defects, only two boojums positioned diametrically at the fibre-droplet surface. Note the similarity between the simulated micrograph (Fig. 5a) and the experimental micrographs in Fig. 2i. For more spherical drops (Fig. 3i) the similarities are partially masked by surface induced curving of cholesteric layers. Both ring structures are also approximately cylindrically symmetric; however, the director field is mostly different in the central region having an additional $-1/2$ disclination ring around the fibre and one (see Fig. 5b) or two (Fig. 5c) surface rings at the fibre surface. A comparison with experimental pictures (Fig. 2iia–c) indicates a close resemblance to the double ring structure (Fig. 5c). For more spherical drops (Fig. 3ii) the similarities are less pronounced due to surface induced curving of cholesteric layers. The ring structures are a compromise between the cylindrical cholesteric layers of the bipolar structure and additional twisting accommodated by the ring defects. This resembles the DSS structure in simple spherical droplets through the toron-like elements (toroidal shaped double-twist cylinders) between the central ring defects and both surface boojums. In the second ring structure, the extra surface ring is thus compensated by the additional cholesteric layer compared to

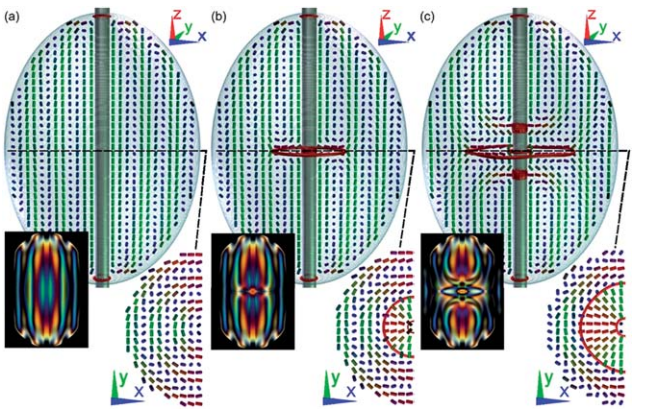

Fig. 5 Numerically calculated structures in cholesteric drops threaded on thin fibres (for $qR = 4\pi$) presented with the director fields in *xz*-plane (top) and *xy*-plane (bottom right), and simulated transmission micrographs (bottom left): (a) the bipolar structure, (b) the ring structure, and (c) the double ring structure. Both (b) and (c) have an additional bulk $-1/2$ disclination ring (red isosurfaces of depressed nematic degree of order) around the fibre in the ring structures. In both ring structures the toron-like elements emerge. Note the resemblance of the simulated micrographs with experiments in Fig. 2.

the first ring structure. All three structures have similar free energies, and their stability largely depends on the material parameters such as the radius-to-pitch ratio and the curvature of the droplet surface (*i.e.* the eccentricity of the ellipsoidal droplets). In a preliminary numerical study we also examined further increase of chirality (shorter pitch). Starting from a bipolar configuration in a given droplet shape we show that by lowering the pitch, ring defects are gradually forming and restructure towards a configuration resembling the diametrical spherical structure.

Here we briefly summarize our numerical modelling. It is based on a continuum Landau-de Gennes approach, where the tensorial order parameter Q_{ij} is used to construct the total free energy as in ref. 30. The free energy minimisation procedure is able to fully characterize (i) the defect regions, *i.e.* the areas with a depressed nematic degree of order, (ii) elastic distortions induced by intrinsic twisting of a cholesteric state, and (iii) the degenerate planar nematic anchoring at the droplet surface. Focusing on the effect of chirality, one-constant elastic approximation is used. The total free energy F is numerically minimized by using an explicit Euler relaxation finite difference scheme on a cubic mesh.[9,31,32] The surface of the droplet is modelled as an ellipsoidal shell of mesh points (with eccentricity 1.25) and the microfibre as a cylindrical shell of mesh points, both with thickness equal to the mesh resolution. To cover the cholesteric twisting of the director and in particular the defects, typically more than 70 mesh points per pitch are used. For material parameters the values typical for a thermotropic cholesteric liquid crystal are used: $L = 4 \times 10^{-11}$ N, $A = -0.172 \times 10^6$ J m^{-3}, $B = -2.12 \times 10^6$ J m^{-3}, $C = 1.73 \times 10^6$ J m^{-3}, $W_0 = 10^{-3}$ J m^{-2}.

To compare the calculated structures with experiments, polarization micrographs of simulated structures are calculated with the Jones 2×2 matrix formalism using $n_o = 1.5$ and $n_e = 1.7$ as ordinary and extraordinary indices of refraction, respectively. The formalism incorporates only the leading contribution – the local variations in birefringence of the nematic refractive index due to the director field – and neglects reflections and refractions at the droplet surface.[33] More specifically, in this formalism, the light beam is propagated along a chosen direction and the total phase shift between ordinary and extraordinary polarisations is accumulated. To reproduce colour images, we repeat the calculation for 10 different wavelengths in an approximate radiation spectrum of a black body at 6000 K (*i.e.* the white light approximation) and sum the results for each wavelength corresponding to RGB colour spectrum weights. The polarization micrographs are calculated for the director structure scaled by a factor of 3 to match the scales of typical experiments and obtain a more quantitative comparison.[34]

Conclusions

We show experimentally generated stable cholesteric liquid crystal microdomains threaded on cellulose fibres that exhibit toroidal topology. The otherwise well-known structures in spherical cholesteric droplets are indeed modified by the presence of piercing cellulose fibres that change both the droplet shape and also topology. Theoretical analysis together with numerical modeling shows possible structures and differences from spherical cholesteric droplets. We demonstrate that the suspended chiral droplets exhibit, for higher twisting power values, a stable disclination ring around the fibre main axis, similar although with the opposite winding number sign to that in suspended nematic droplets with homeotropic anchoring.

The experimental system presented in this work is highly sensitive to temperature variations resulting in structural changes, which opens new possibilities for the production of enhanced "weightless" web-like thermo-optical devices. Such web-like mats based on electro-spun micro/nanocellulose fibres could therefore make also an ideal system for the detailed studies of liquid crystal microdroplets suspended in air. Moreover, the incorporated cellulose thread inherently connected to the liquid crystal-director and defect-structure could possibly couple these systems to diverse external fields, making such systems potentially useful for tunable photonic and waveguide applications.

Acknowledgements

D.S. and S.Ž. acknowledge the ARRS program P1-0099 and the Center of Excellence NAMASTE. D.S. is thankful to Simon Čopar for the help with visualization of numerical results. This work was partially supported by the Portuguese Science and Technology Foundation grant SFRH/BD/63574/2009 and projects PTDC/CTM-POL/1484/2012, PTDC/FIS/110132/2009, and PEst-C/CTM/LA0025/2011 (Strategic Project – LA 25-2011-2012). O.D.L. is thankful for the support of NSF DMR 1104850 grant.

Notes and references

1 I. Ilchishin, E. Tikhonov, V. Tishchenko and M. Shpak, *JETP Lett.*, 1980, **32**, 24–27.
2 H. Coles and S. Morris, *Nat. Photonics*, 2010, **4**, 676–685.
3 A. D. Ford, S. M. Morris and H. J. Coles, *Mater. Today*, 2006, **9**, 36–42.
4 G. E. Volovik and O. D. Lavrentovich, *Zhurn. Eksp. Teor. Fiz.*, 1983, **85**, 1997–2010; G. E. Volovik and O. D. Lavrentovich, *Sov. Phys. JETP*, 1958, 1159–1166 (1983).
5 S. Kralj and S. Žumer, *Phys. Rev. A: At., Mol., Opt. Phys.*, 1992, **45**, 2461.
6 M. Humar and I. Muševič, *Opt. Express*, 2011, **19**, 19836–19844.
7 M. Humar, M. Ravnik, S. Pajk and I. Muševič, *Nat. Photonics*, 2009, **3**, 595–600.
8 J. Bezić and S. Žumer, *Liq. Cryst.*, 1992, **11**, 593–619.
9 D. Seč, T. Porenta, M. Ravnik and S. Žumer, *Soft Matter*, 2012, **8**, 11982–11988.
10 G. Cipparrone, A. Mazzulla, A. Pane, R. J. Hernandez and R. Bartolino, *Adv. Mater.*, 2011, **23**, 5704.
11 D. J. Gardiner, W. K. Hsiao, S. M. Morris, P. J. W. Hands, T. D. Wilkinson, I. M. Hutchings and H. J. Coles, *Soft Matter*, 2012, **8**, 9977–9980.
12 M. Humar and I. Muševič, *Opt. Express*, 2010, **18**, 26995–27003.
13 J. Doane, N. Vaz, B. G. Wu and S. Žumer, *Appl. Phys. Lett.*, 1986, **48**, 269–271.

14 D. J. Gardiner, S. M. Morris, P. J. Hands, C. Mowatt, R. Rutledge, T. D. Wilkinson and H. J. Coles, *Opt. Express*, 2011, **19**, 2432–2439.
15 T. Lopez-Leon, V. Koning, K. B. S. Devaiah, V. Vitelli and A. Fernandez-Nieves, *Nat. Phys.*, 2011, **7**, 391.
16 B. Senyuk, Q. Liu, S. He, R. D. Kamien, R. B. Kusner, T. C. Lubensky and I. I. Smalyukh, *Nature*, 2013, **493**, 200–205.
17 Y. Geng, P. L. Almeida, J. L. Figueirinhas, E. M. Terentjev and M. H. Godinho, *Soft Matter*, 2012, **8**, 3634–3640.
18 E. Terentjev, *Nat. Mater.*, 2013, **12**, 187–189.
19 G. Gray and D. McDonnell, *Mol. Cryst. Liq. Cryst.*, 1976, **37**, 189–211.
20 P. Sebastião, A. Gradišek, L. Pinto, T. Apih, M. Godinho and M. Vilfan, *J. Phys. Chem. B*, 2011, **115**, 14348–14358.
21 M. Godinho, J. Canejo, G. Feio and E. Terentjev, *Soft Matter*, 2010, **6**, 5965–5970.
22 N. Mori, M. Morimoto and K. Nakamura, *Macromolecules*, 1999, **32**, 1488–1492.
23 M. V. Kurik and O. D. Lavrentovich, *Mol. Cryst. Liq. Cryst.*, 1982, **72**, 239–246.
24 F. Xu and P. Crooker, *Phys. Rev. E: Stat. Phys., Plasmas, Fluids, Relat. Interdiscip.Top.*, 1997, **56**, 6853.
25 P. De Gennes and J. Prost, *The Physics of Liquid Crystals*, Oxford University Press, Oxford, 1993.
26 C. Robinson, J. Ward and R. Beevers, *Discuss. Faraday Soc.*, 1958, **25**, 29–42.
27 M. A. Gharbi, D. Seč, T. Lopez-Leon, M. Nobili, M. Ravnik, S. Žumer and C. Blanc, *Soft Matter*, DOI: 10.1039/C3SM00126A.
28 O. D. Lavrentovich, *Liq. Cryst.*, 1998, **24**, 117–126.
29 O. D. Lavrentovich and L. N. Tarakhan, *Poverkhnost*, 1990, **1**, 39–44.
30 M. Ravnik, G. P. Alexander, J. M. Yeomans and S. Žumer, *Faraday Discuss.*, 2010, **144**, 159–169.
31 M. Ravnik and S. Žumer, *Soft Matter*, 2009, **5**, 269–274.
32 M. Ravnik and S. Žumer, *Liq. Cryst.*, 2009, **36**, 1201–1214.
33 R. Ondris-Crawford, E. P. Boyko, B. G. Wagner, J. H. Erdmann, S. Žumer and J. W. Doane, *J. Appl. Phys.*, 1991, **69**, 6380–6386.
34 M. K. McCamley, G. P. Crawford, M. Ravnik, S. Žumer, A. W. Artenstein and S. M. Opal, *Appl. Phys. Lett.*, 2007, **91**, 141916.